High-resolution hot-film measurement of surface heat flux to an impinging jet

High-resolution hot-film measurement of surface heat flux to an impinging jet

2011 Meas. Sci. Technol. 22 105402

(http://iopscience.iop.org/0957-0233/22/10/105402)

Meas. Sci. Technol. **22** (2011) 105402 (11pp) doi:10.1088/0957-0233/22/10/105402

High-resolution hot-film measurement of surface heat flux to an impinging jet

T S O'Donovan[1], T Persoons[2] and D B Murray[2]

[1] School of Engineering and Physical Sciences, Heriot-Watt University, Edinburgh EH14 4AS, UK
[2] Mechanical and Manufacturing Engineering, Trinity College Dublin, Dublin 2, Ireland

E-mail: T.S.O'Donovan@hw.ac.uk

Received 23 February 2011, in final form 4 July 2011
Published 19 August 2011
Online at stacks.iop.org/MST/22/105402

Abstract

To investigate the complex coupling between surface heat transfer and local fluid velocity in convective heat transfer, advanced techniques are required to measure the surface heat flux at high spatial and temporal resolution. Several established flow velocity techniques such as laser Doppler anemometry, particle image velocimetry and hot wire anemometry can measure fluid velocities at high spatial resolution (μm) and have a high-frequency response (up to 100 kHz) characteristic. Equivalent advanced surface heat transfer measurement techniques, however, are not available; even the latest advances in high speed thermal imaging do not offer equivalent data capture rates. The current research presents a method of measuring point surface heat flux with a hot film that is flush mounted on a heated flat surface. The film works in conjunction with a constant temperature anemometer which has a bandwidth of 100 kHz. The bandwidth of this technique therefore is likely to be in excess of more established surface heat flux measurement techniques. Although the frequency response of the sensor is not reported here, it is expected to be significantly less than 100 kHz due to its physical size and capacitance. To demonstrate the efficacy of the technique, a cooling impinging air jet is directed at the heated surface, and the power required to maintain the hot-film temperature is related to the local heat flux to the fluid air flow. The technique is validated experimentally using a more established surface heat flux measurement technique. The thermal performance of the sensor is also investigated numerically. It has been shown that, with some limitations, the measurement technique accurately measures the surface heat transfer to an impinging air jet with improved spatial resolution for a wide range of experimental parameters.

Keywords: hot film, surface heat flux, jet, impingement

(Some figures in this article are in colour only in the electronic version)

Nomenclature

A	area (m^2)
D	jet diameter (m)
h	convective heat transfer coefficient (W m^{-2} K^{-1})
I	current (A)
k	thermal conductivity (W m^{-1} K^{-1})
Nu	Nusselt number (hD/k)
Pr	Prandtl number
q	heat (W)
q''	heat flux (W m^{-2})
R	resistance (Ω)
Re	Reynolds number ($\rho UD/\mu$)
T	temperature (K)
U	jet exit velocity (m s^{-1})
V	voltage (V)

Subscripts

eff	effective
geo	geometric

1. Introduction

Advanced surface heat flux and fluid flow measurement techniques are required to further the understanding of the complex coupling between local flow velocities and the adjacent surface heat flux in convective heat transfer applications. Several fluid velocity measurement techniques exist that can measure flow velocities in three dimensions and at high spatial and temporal resolution. For example, laser Doppler anemometry (LDA) can measure the speed of seeding particles of the order of 1 μm in a fluid flow at a rate in excess of 100 kHz (Albrecht *et al* [1]). Particle image velocimetry has also been developed to the stage where it can measure a velocity flow field at a rate of 10 kHz and to μm level resolution (Raffel *et al* [2]). Even before the advent of laser flow measurement techniques hot-wire anemometry, as described by Bruun [3], was capable of measuring fluid velocities in the MHz range with good spatial resolution (approximately 100 μm).

Surface heat flux measurement technology has not kept pace with developments of fluid velocity measurement techniques. Thermocouples, thermochromic liquid crystals (TLCs) and infrared thermal imaging all measure temperature and when applied to a uniform wall heat flux boundary condition the surface heat transfer coefficient can be calculated. Even the state-of-the-art of these technologies is not comparable to standard flow measurement technologies. Fine wire thermocouples have a maximum-frequency response rate in the region of 330 Hz (Ireland and Jones [4]); TLCs have a much lower frequency response rate and a narrow operating temperature range (normally 5–15 K). High-speed infrared thermal imaging and pyrometry are the latest advancements in heat transfer measurement technology and can measure surface temperatures in the kHz region. Golobic *et al* [5] have employed thermal imaging for a transient measure of surface heat flux to a two-phase flow. In this case however, the Biot number is high and the transients are slow. For time varying signals due to turbulent flows, where the amplitude of the fluctuations is low relative to the magnitude, simple energy balance equations are insufficient for the calculation of the time varying surface heat flux signal.

The thickness, thermal conductivity and heat capacitance of the surface (usually a thin foil) will all need to be considered in calculations of the surface heat flux. In the case of infrared thermal imaging, high-frequency imaging does not directly equate to high-speed surface flux measurements, no more than it does for surfaces coated in TLCs. A study by Nakamura [6], however, has shown that the maximum surface heat flux frequency detectable using thermal imaging of very thin foils (2–10 μm) is still in the range of 100 Hz when used in air flows. While this falls short of what is available in fluid flow measurements, this is a very useful advancement in the technology and is likely to aide many convective heat transfer measurement investigations. A further disadvantage of the heat transfer measurement technology discussed so far is their exclusive applicability to uniform wall flux (UWF) surfaces. These technologies cannot be used for uniform wall temperature conditions to calculate the surface heat flux.

To address the need for an accurate surface heat flux measurement technique with high spatial and temporal resolution, the use of a flush-mounted hot film for surface heat flux measurement is under investigation. It is applied in an impinging jet flow as this is an established area that would nevertheless benefit from the improvement in understanding brought about by higher-resolution data. Impinging jet flows are a very effective means of achieving high rates of surface heat transfer. For this reason, they are employed in several heat transfer applications including turbine blade and electronics cooling.

An early study of jet impingement heat transfer was conducted by Hoogendoorn [7] where the effect of jet exit turbulence on the stagnation point heat transfer was investigated. Gardon and Akfirat [8] also conducted a study of the role of turbulence in jet impingement heat transfer; both studies inferred the effect that velocity fluctuations had on the mean surface heat transfer. Research in this area has been extensive and more recently the measurement of surface heat transfer fluctuations to an impinging jet flow has given new insight into the convective heat transfer mechanisms. Liu and Sullivan [9] used a hot-film sensor to measure time varying surface heat flux signal to an impinging air jet. While the technique used by Liu and Sullivan [9] measured the magnitude of the surface heat flux fluctuations accurately, the mean surface heat flux was measured by other means.

O'Donovan and Murray [10, 11] investigated the effect of vortices, that occur naturally in an impinging jet flow, on the surface heat transfer for jets impinging at low nozzle to surface spacings. By mounting a hot film on the impingement surface, the time varying surface heat flux signal was acquired but needed to be referenced to a separate measure of the mean surface heat flux. This approach led to the finding that as vortices break down in the wall jet, the surface heat transfer is enhanced to form a secondary peak at a radial location.

The use of flush-mounted hot-film sensors to measure surface heat flux therefore is not new. Xie and Wroblewski [12] used a hot film to study the time-resolved heat flux downstream of a cylinder–wall junction. Beasley and Figiola [13] developed a technique to calibrate the sensor. It was found that the effective surface area of the sensor can vary from 1 to 10 times the geometric surface area depending on the operating parameters and the magnitude of the surface heat flux. Moen and Schneider [14] investigated the frequency response for a hot-film sensor which is reported to be approximately 100 kHz for similar nickel sensor elements. Moen and Schneider [14] also found that the frequency response increased with larger values of sensor overheat.

Since a hot film must operate at a temperature above that of the surface, this sensor overheat introduces an error in the surface heat flux signal. A correction for the sensor overheat was first presented by Scholten and Murray [15] for a heated cylinder in cross-flow. It was found that the technique is only valid for the attached flow regime within a range from 0° (front stagnation point) to 100° (boundary layer separation point). As the thermal performance of the sensor is still not fully understood, it is not widely employed in experimental investigations; an objective of the current research is to go some way towards addressing this shortcoming.

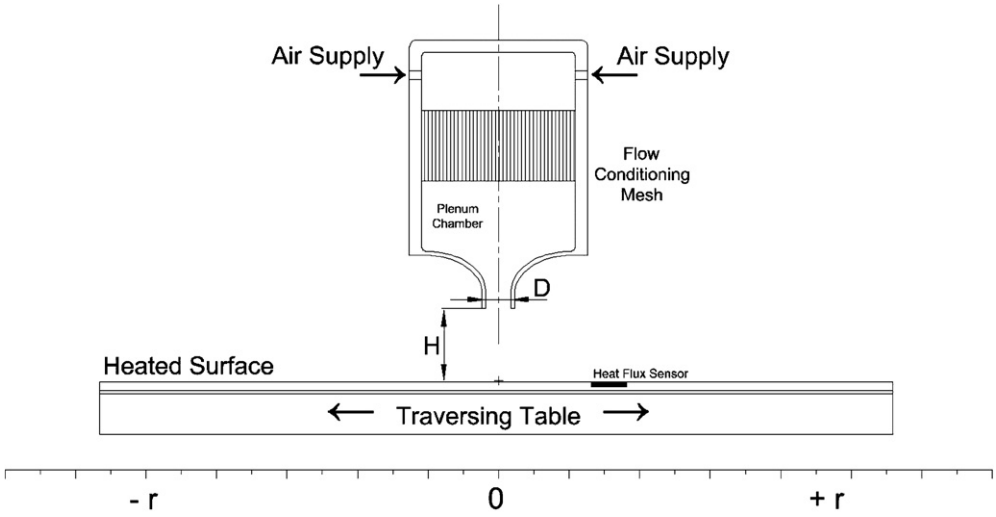

Figure 1. Experimental test rig.

Several investigators have used excitation techniques to further increase the localized and area averaged heat transfer. Examples of such studies are those reported by Hwang *et al* [16] and Hwang and Cho [17]; an acoustic speaker was employed in these studies to control the naturally occurring vortices within the flow. Excitation at a sub-harmonic of the natural frequency for example, encouraged vortex merging and influenced the jet spread rate. This in turn affected the surface heat transfer. Similar to earlier studies however, the influence of the acoustic excitation on the resulting surface heat transfer is only inferred. Local and temporally simultaneous velocity and surface heat transfer measurements at frequencies of the same order of magnitude as the excitation frequencies would give greater insight into the effect of the excitation of the surface heat transfer.

For these reasons, it is important that enhanced surface heat transfer techniques are developed. New insight into convective heat transfer mechanisms in periodic and aperiodic flows will lead to overall enhancement of cooling technology performance. The effect of these techniques on the surface heat transfer can only be understood by analysing the surface heat transfer at high spatial and temporal resolution. The use of a hot film that is flush mounted on the heated impingement surface is investigated in the current research. Although the response time of the sensor has the potential to improve the temporal resolution for surface heat flux measurements, the current study is concerned with measuring the time-average surface heat flux. The calibration of the sensor and details of the measurement technique are presented.

2. Experimental rig

The experimental rig is similar to that used in studies by O'Donovan and Murray [10, 11] and is illustrated in figure 1. A 5 mm thick copper plate is electrically heated from below and approximates a uniform wall temperature boundary condition. Air is supplied to the jet nozzle chamber though four separate inlets from the building compressors via a large plenum chamber to eliminate flow fluctuations. Two filters are also connected on the compressed air line to extract all trace of moisture and impurities from the air. An MKS mass flow controller (model 1579 A) is installed on the compressed air line to regulate the jet exit Reynolds number. The meter is rated up to 300 litres per minute and has an accuracy of 1% of full scale. The air flows though a dense mesh before exiting though the contoured nozzle which forms a jet that is directed at the heated impingement surface. The 13 mm diameter jet is held above the heated surface in a clamp, the height of which can be varied from 0.5 to 10 jet diameters above the heated surface.

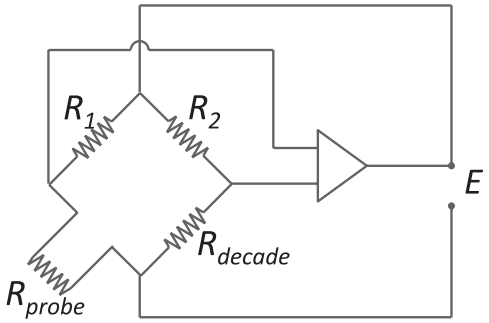

Figure 2. CTA circuitry.

The heated impingement surface is instrumented with two flush-mounted sensors. The first, and the subject of this investigation, is a flush-mounted hot-film sensor supplied by Tao Systems. The sensor consists of a nickel sensor element that is electron beam deposited onto a 51 μm thick Upilex S polyimide film. The hot-film element has a thickness of $<$0.2 μm and covers an area of approximately 100 μm $\times$ 1400 μm. Copper leads that have a resistance of approximately 0.002 Ω mm^{-1} are also deposited on the film to provide terminals for connection to the constant temperature anemometer (CTA). A Dantec 90C10 Streamline CTA module is used in the current investigation and the sensor is connected to the CTA with a 1 m long BNC cable. The hot-film sensor element, together with the sensor cables, forms one arm of a Wheatstone bridge as indicated by R_{probe} in figure 2; the

temperature of the sensor can be adjusted by setting the decade resistance on another arm.

The second surface heat flux sensor, an RdF Micro-Foil®, is also flush mounted on the impingement surface. This sensor consists of two thermopiles located above and below a Kapton thermal barrier. The voltage produced by the differentially coupled thermopiles is therefore proportional to the heat flux through the sensor. The sensor thickness is relatively small (approximately 200 μm), and therefore one-dimensional conductive heat transfer through the sensor is assumed equal to the convective surface heat flux. As the voltage produced by the sensor is also small, the signal is amplified by a factor of 1000 with a Fylde differential dc amplifier before acquisition. This sensor has a relatively large surface footprint (6 × 10 mm), even though the thermopiles are a small fraction of this area and are located at one end of the sensor. During testing, the sensor is positioned such that the thermopiles are at the leading edge to reduce the effect of the disturbance of the thermal boundary condition on the measurement. The disturbance caused to the thermal boundary condition and the consequence for the surface heat transfer measurements are discussed in the results section. The response time of the sensor provided by the manufacturer is 0.01 s to reach 62% of a step input. For the range of turbulent jet Reynolds numbers investigated (10 000–30 000) velocity fluctuations occur in the kHz region, and therefore the RdF Micro-Foil® heat flux sensor is inadequate for this purpose but can provide accurate time and spatially averaged results.

The temperature of the heated surface is monitored by two thermocouples. One is positioned directly below the hot-film sensor and the second is embedded in the Micro-Foil® heat flux sensor. While the thermal boundary condition approximates a uniform wall temperature, the local temperature is used in calculations to account for minor temperature variations across the heated surface. Because all sensors are point measurement techniques, both the jet clamp and the heated impingement surface are mounted on orthogonal tracks. Therefore, to achieve profiles of the surface heat transfer, the sensors can be placed in the impinging jet flow at any point in a two-dimensional plane extending beyond 6 diameters from the jet's geometric centre.

3. Theory

A CTA maintains the hot-film sensor element at a constant resistance and hence a constant sensor temperature. The sensor element is set to an elevated temperature above that of the surrounding impingement surface. Hereafter, this difference in temperature will be referred to as the sensor overheat. The power required to maintain the sensor at this temperature can be related to the surface heat flux. Ideally, to maintain a uniform wall temperature boundary condition and to reduce errors associated with conductive losses, the sensor would be maintained at a temperature equal to the heated surface. If this were the case however, no electrical power would be required to maintain its temperature as this would be supplied from the heated surface. Therefore, to acquire a signal, it is necessary to overheat the sensor. The power required to maintain the sensor overheat temperature is equal to the heat losses from the sensor; these include convective heat losses to the air flow and conduction to the heated surface. Therefore, a balance must be found, where the overheat is sufficiently large to produce a significant signal (to maximize signal to noise ratio) but small enough so that errors can be easily quantified and corrected for as part of the measurement technique.

Part of the calibration procedure is to determine the effective surface area of the sensor. The power, or energy dissipated, ($q_{\text{dissipated}}$) from the film can be calculated from the measurement of the voltage required to maintain the sensor at a certain temperature as shown:

$$q_{\text{dissipated}} = \frac{R_{\text{film}}}{(R_1 + R_{\text{probe}})^2} \times E^2, \tag{1}$$

where the probe resistance is the sum of the film and cable resistances.

Thus, the heat from the sensor can be calculated from sensor properties and the time-varying measurement of the CTA top bridge voltage.

Heat from the sensor element also conducts to the surrounding substrate and sensor leads; this increases the effective surface area (A_{eff}) of the sensor. Therefore, in order to calculate the surface heat flux, the effective surface area must be calibrated against an established reference heat flux measurement. There is a high degree of variability in heat transfer correlations for an impinging air jet. This is largely due to dissimilarities in the jet flow characteristics. For otherwise similar experimental setups (i.e. Reynolds number, nozzle to impingement surface spacing and thermal boundary condition) correlations by Gardon and Akfirat [8] give very different results to those achieved by Goldstein and Franchett [18] for example. The current setup is calibrated with reference to a correlation (equation (2)) developed by Liu and Sullivan [9] and based on a potential flow analysis by Shadlesky [19]. Equation (2) is valid for the surface heat transfer at the stagnation point, at low nozzle to impingement surface spacings. It has been verified against experimental measurements by Liu and Sullivan [9] for nozzle to impingement surface spacing less than 2 diameters and jet exit Reynolds numbers from 12 000–15 000. This correlation was chosen as it was in good agreement with the manufacturer's independent calibration of the Micro-Foil® heat flux sensor and also limits the experimental variables such as the effects of jet spread and the entrainment of ambient fluids as it is only valid at the stagnation point and at nozzle to impingement surface spacings that lie within the core of the jet:

$$Nu = 0.585 Pr^{0.4} Re^{0.5}. \tag{2}$$

By combining equations (1) and (2) with Newton's law of cooling, the effective surface area can be calculated as

$$A_{\text{eff}} = \frac{R_{\text{film}} E^2 D}{0.585(R_1+R_{\text{film}}+R_{\text{cable}})^2 (T_{\text{surface}}-T_{\text{jet}}) k_{\text{fluid}} \,\text{Pr}^{0.4}\, Re^{0.5}}. \tag{3}$$

The above characterization of the sensor effective surface area works only in ideal circumstances where the sensor overheat is zero. As discussed earlier, in the absence of an appreciable overheat the technique would not yield a measurement signal.

It is therefore necessary to apply a significant overheat to acquire a signal and then to correct for the offset or bias error that the overheat introduces to the measurement signal. This third part of the calibration procedure outlines the steps taken to measure the bias error to correct the raw measurement.

Power from the sensor is a combination of convective heat transfer from the film to the jet flow and conductive losses to the heated surface. Convective heat transfer is overestimated as the temperature of the film is higher than the temperature of the impingement surface surrounding the sensor. Heat is also conducted to the surface because of the elevated hot-film temperature. These factors contribute to a bias error in the raw measurement. Both are difficult to estimate as the proportion of the bias error due to convection requires foreknowledge of the convective heat transfer coefficient. And the proportion of the bias error attributed to the conduction depends on precise measurements of the sensor geometry and material properties. This can be further complicated by the use of adhesives when mounting the sensor on the impingement surface. Therefore, another method is required to estimate the bias error before the surface heat flux can be accurately established.

To accurately measure the bias error in the raw measurement, two tests are conducted. For the same sensor overheat, jet positioning and Reynolds number, measurements are made under heated and adiabatic conditions. In the adiabatic test, the impingement surface and jet air temperatures are maintained at ambient temperature. The sensor heat flux ($q_{\text{adiabatic}}$) is equal to the sum of convection and conduction from the sensor based on the overheat temperature difference as indicated in the following equation:

$$q_{\text{adiabatic}} = q_{\text{cond}_{\Delta T=OH}} + q_{\text{conv}_{\Delta T=OH}}. \tag{4}$$

In the heated test, the impingement surface is held at a temperature above that of the ambient and impinging air jet. The sensor heat flux (q_{heated}) also includes a conduction term, again based on a temperature difference equal to the overheat, and a convection term as indicated in the following equation:

$$q_{\text{heated}} = q_{\text{cond}_{\Delta T=OH}} + q_{\text{conv}_{\Delta T=OH+T_{\text{surf}}-T_{\text{air}}}}. \tag{5}$$

The convection term is overestimated as it is based on the temperature difference between the sensor and the air ($\Delta T = OH + T_{\text{surf}} - T_{\text{air}}$). Therefore, assuming the convective heat flux is linear with the temperature difference, subtracting the heat flux from the sensor during adiabatic conditions from the heat flux during heated conditions results in a measure of the surface heat flux based on the temperature difference between the surface temperature and the jet temperature:

$$q_{\text{conv}_{\Delta T=T_{\text{surf}}-T_{\text{air}}}} = q_{\text{heated}} - q_{\text{adiabatic}}. \tag{6}$$

In theory, therefore, this method can be applied for any overheat value. In practice however, as will be discussed in the next session, it is still of benefit to minimize the overheat as this, in turn, reduces the disturbance of the thermal boundary condition.

4. Results and discussion

This section demonstrates the hot-film surface heat flux measurement technique for an impinging air jet. Firstly, the sensor calibration technique is analysed for the range of parameters tested. This is then compared to a numerical simulation of the sensor's thermal performance. Finally, the results attained with the hot-film technique are compared to those determined by using a more established measurement technique.

4.1. Calibration of the hot-film sensor

As indicated in the experimental rig section, a thin unshielded T-type thermocouple is embedded in the heated surface directly below the hot-film sensor element. During calibration, a second thermocouple was positioned above the sensor element and the whole system was insulated with fibreglass wool. The plate was then electrically heated to approximately 100 °C and allowed to cool slowly under the control of the heating element; the apparatus was deemed to have reached a steady state when the temperature above and below the hot-film fell within 0.1 K. At each temperature setting, the resistance of the hot-film probe was measured by balancing the bridge with the decade resistance. This ensured that the probe was calibrated *in situ* while connected to the CTA. As expected, a linear relationship was found between the probe resistance and temperature as shown in the following equation:

$$R_{\text{film}} = R_{\text{film},0}(1 + \alpha_0(T_{\text{film}} - T_0)), \tag{7}$$

where the temperature coefficient of resistance $\alpha_0 = 0.357\%$ K^{-1} and the reference film resistance, $R_{\text{film},0} = 7.488\ \Omega$ at a the reference temperature, $T_0 = 293.15$ K.

Both the uncertainty in the regression curve and the precision of the measurement are less than 0.1% for the entire operating temperature range of the sensor. The cable resistance was measured by shorting the lead terminals and balancing the Wheatstone bridge; it was found to be 0.8 Ω.

Since the hot film is maintained at an elevated temperature above the heated surface, heat from the hot-film element will conduct to the substrate, increasing the temperature of the substrate locally. The temperature of the substrate will decrease with distance from the film to the impingement surface temperature. The affected area is equivalent to a smaller area at the overheat temperature, which is defined as the effective surface area. The effective surface area is therefore defined mathematically as

$$A_{\text{eff}} = \frac{\int (T - T_{\text{substrate}})\,\mathrm{d}A}{T_{\text{film}} - T_{\text{substrate}}}. \tag{8}$$

The area in question is the area where the temperature has been elevated above the surrounding by the presence of the films overheat. A series of tests were conducted where the hot-film sensor was positioned at the stagnation point of a jet impinging at a nozzle to impingement surface spacing of 2 diameters. The jet Reynolds number was varied from 10 000 to 30 000 and the sensor overheat was also varied from 3 to 15 K.

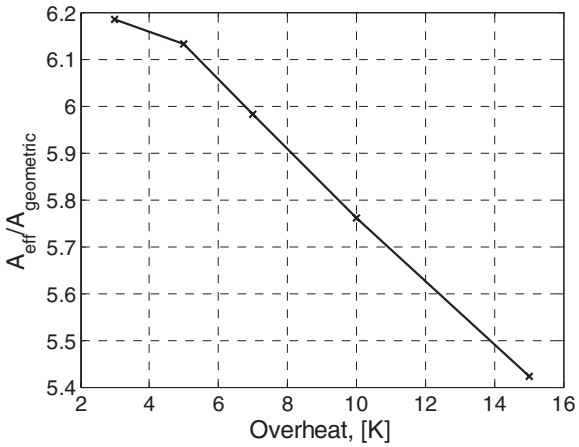

Figure 3. Effect of overheat on effective surface area.

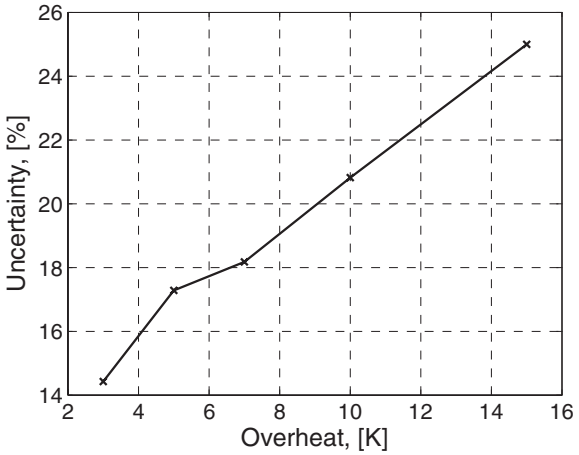

Figure 4. Uncertainty of effective surface area calibration.

The effective surface area is calculated from the CTA signal using equation (3) and was found to vary almost linearly from 6.2 to 5.4 times the actual or geometric surface area of the film as the overheat was increased from 3 to 15 K (figure 3).

The uncertainty interval for the effective surface area is defined as the band about the reported result within which the true value is expected to lie with 95% confidence; this is in accordance with Kim *et al* [20]. The uncertainty is calculated from the precision limit which is defined as two times the standard deviation of a measurement when based on at least 30 samples. The bias limit does not contribute to the overall uncertainty in this instance as it is calibrated against a reference correlation (Shadlesky [19]). Figure 4 shows that the uncertainty of the effective surface area varies with the sensor overheat, from 14% to 25% for the range of overheats tested.

As the overheat increases so too does the uncertainty; large overheats disturb the thermal boundary condition more. Although the effective surface area is smaller in this case, the area affected by the hot-film sensor is greater. For the range of parameters tested therefore, lower values of sensor overheat are preferable. As the magnitude of the overheat approaches zero however, it is anticipated that the uncertainty would increase again. The power required to maintain the sensor overheat at a low overheat would be small, thus the voltage signal would decrease leading to an insignificant signal-to-noise ratio.

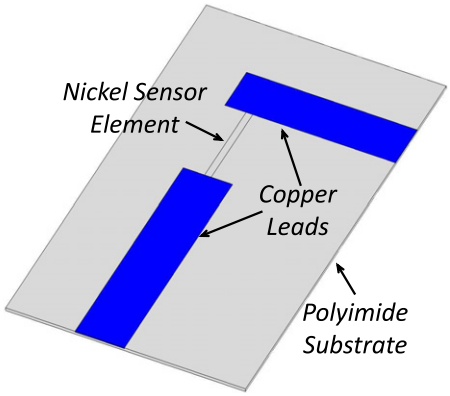

Figure 5. Model of sensor geometry.

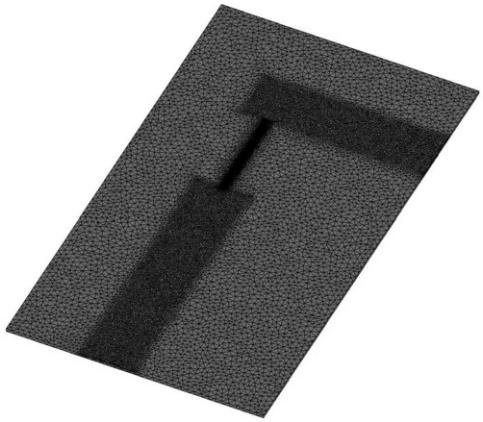

Figure 6. Numerical model mesh.

4.2. Numerical analysis

To gain a greater insight into the thermal performance of the hot-film sensor, a numerical model was constructed in COMSOL Multi-physics. The temperature distribution throughout the geometry of the sensor was investigated in both hot and cold (adiabatic) conditions. The thermal model consisted of the nickel sensor element, copper leads and polyimide substrate as illustrated in figure 5. The dimensions of the sensor were supplied by Senflex and faithfully modelled in three dimensions. The mesh of the numerical model is illustrated in figure 6. In excess of 125 thousand prism elements were used in the mesh and it was concentrated in the regions of highest thermal gradients as indicated.

A uniform wall temperature boundary condition was applied beneath the substrate of the hot film equal to the impingement surface temperature. A uniform convective heat transfer coefficient determined by the correlation proposed by Shadlesky [19] was applied from the surface of the hot-film sensor element and substrate for each test Reynolds number. The surface temperature of the Nickel hot-film sensor element

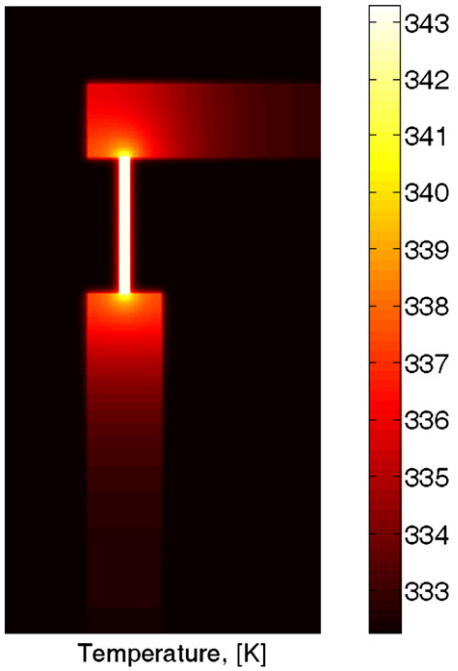

Figure 7. Hot-film sensor temperature distribution: $Re = 20\,000$ and overheat = 10 K.

was set equal to the sum of the surface temperature and the overheat temperature.

The resulting temperature distribution over the surface of the hot film, where a surface heat transfer coefficient is 145 W m^{-2} K^{-1} is presented in figure 7. This is the equivalent stagnation point heat transfer coefficient reached by a jet ($Re = 20\,000$) where the impingement surface is placed within the jet core.

Heat from the film, which is at a temperature varying between 3 and 15 K above that of the surrounding surface, is conducted to the sensor substrate and copper leads. The temperature distribution shown in figure 7 indicates that heat from the nickel sensor element is conducted primarily to the attached copper leads. This has the effect of increasing the surface area substantially but also non-uniformly. The heated surface area extends along the copper leads to a distance of more than twice its geometric length, which reduces the spatial resolution of the technique. Variable heat capacitance and conductivity of the copper, nickel and polyimide substrate will also influence the response time of the measurement technique.

The magnitude of the effective surface area is plotted as a function of the sensor overheat in figure 8 for a hot and cold test. It can be seen that the effective surface area is close to constant for the whole range of overheats in the adiabatic test. For the hot test however, the effective surface area is overall larger and decreases with increasing magnitude of the overheat. This is broadly in line with the experimental findings presented earlier in figure 3. For the experimental case however, it is not possible to determine a separate surface area for both the adiabatic and heated case and the effective surface area reported is a weighted average of the two. The numerical results clearly show that there is a discrepancy here and this is likely to have contributed to the uncertainty values reported in figure 4.

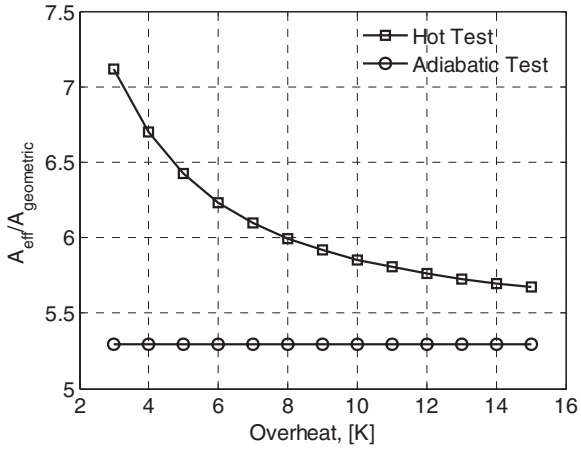

Figure 8. Effective surface area: $Re = 20\,000$.

4.3. Heat transfer to an impinging air jet

To demonstrate the technique, heat transfer to an impinging air jet for a range of experimental parameters was measured using the hot-film sensor. The hot film was initially positioned at the stagnation point of the impinging air jet; the temperature was allowed to reach steady state and the decade resistance was set to achieve a hot-film temperature equal to the sum of the impingement surface temperature and the overheat. The impingement surface, which can be positioned relative to the jet was then moved so that the sensor was located at the required radial location. This procedure was then repeated until a full profile of the heat flux from the surface to the impinging air jet was acquired. It was also repeated for heated and adiabatic tests for otherwise identical experimental conditions. An example of the results is presented in figure 9 for a jet Reynolds number of 10 000, with the nozzle positioned 1 diameter distant from the impingement surface and for a range of overheats from 3 to 15 K.

Both the heated and adiabatic tests result in similar surface heat flux distributions. The heat flux is a local minimum at the stagnation point and rises to a peak at a radial location of approximately 0.75D. It then decreases before rising to a second and third peak at radial distances of 1.3D and 2.5D approximately. The peaks are less pronounced in the adiabatic test and the third radial peak is not discernable in these profiles. It is also apparent that the overall magnitude of the surface heat flux is lower for low values of the overheat. This is due to the small temperature differential between the hot film and the air jet or impingement surface. While low values of surface heat flux will result in higher values of measurement uncertainty, higher values result in a higher bias error as the sensor itself can introduce a significant disturbance in the thermal boundary condition.

To determine the actual surface heat flux by convection to the impinging air jet, the adiabatic value of the surface heat flux is subtracted from the heated test value in accordance with equation (6). The distribution of the Nusselt number has been determined for the data presented in figure 9 where the temperature differential is the difference between the impingement surface temperature (T_{surf}) and the jet air

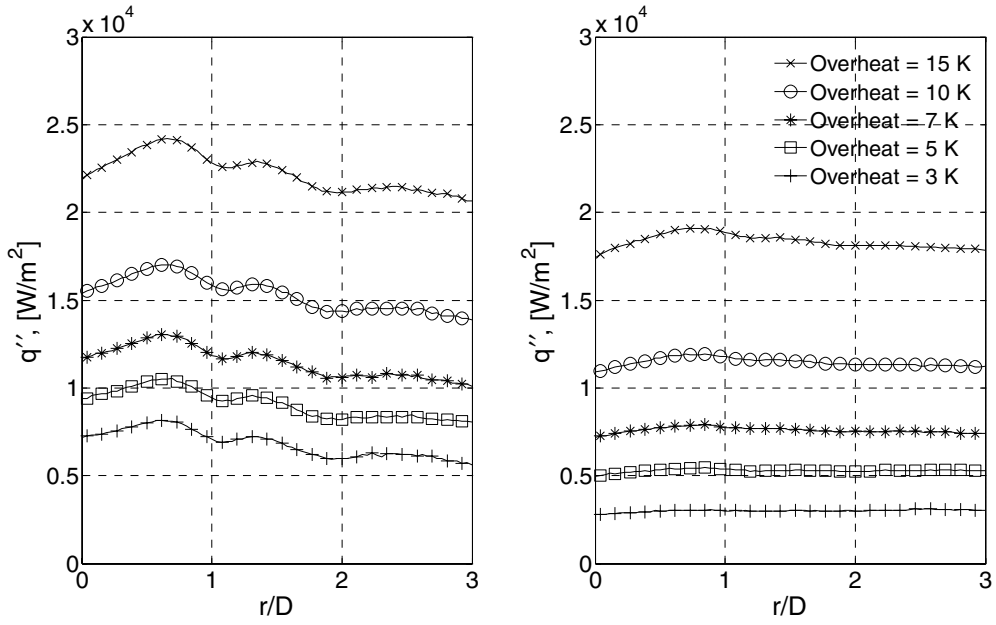

(*a*) **Heated Test** (*b*) **Adiabatic Test**

Figure 9. Distribution of heat flux to a jet impinging at $Re = 10\,000$ and $H/D = 1.0$: (*a*) heated test and (*b*) adiabatic test.

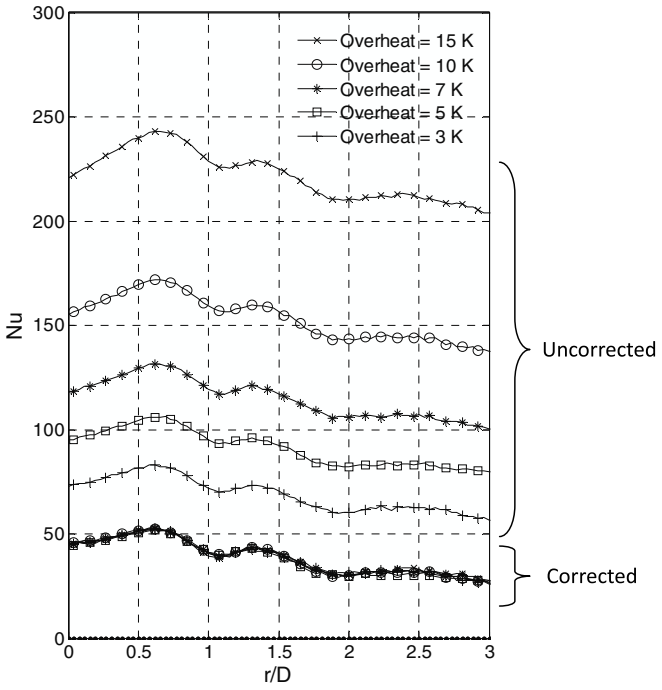

Figure 10. Effect of overheat on Nusselt number distributions: $Re = 10\,000$ and $H/D = 1.0$.

temperature. Both corrected and uncorrected results are presented in figure 10.

It is apparent, from figure 10, that the magnitude of the sensor overheat has a significant influence on the magnitude of the uncorrected Nusselt number distributions. Once the correction technique has been applied however, it can be seen from figure 10 that the data are in agreement to within 2%. The shape of the Nusselt number distribution is consistent with results published by Gardon and Akfirat [8], Goldstein *et al* [16], Baughn *et al* [21] and others in the range from $r/D = 0$–2.

Beyond $r/D = 2$, however, the Nusselt number distribution exhibits a peak at approximately $r/D = 2.5$; this is more apparent for the results presented in figure 11 for $Re = 10\,000$. This third peak in the Nusselt number distribution is inconsistent with results presented in the literature; it is therefore considered to be an artefact of the measurement technique. The magnitude of this tertiary peak increases with increasing overheat and therefore it is possible that it is due to artificial enhancement from natural or buoyancy-driven convection which, at these relatively large radial locations and low local velocities, is at par with the forced convection. A similar finding was presented by Scholten and Murray [15] for a cylinder in crossflow. The overheat correction technique was shown to breakdown at an angular position of 100° from the front stagnation point (0°). This was attributed by Scholten and Murray [6] to separation of the boundary layer; however, this is also a location of low forced convective heat transfer. To further investigate this apparent limitation of the measurement technique, further tests were conducted at higher Reynolds number values.

Heat transfer distributions to an otherwise similar jet were investigated for Reynolds numbers of 20 000 and 30 000 and overheats of 5 K and 10 K, respectively. The results are presented in figure 11. These data are in agreement to within 6% which is much less than the uncertainty values reported in figure 4. It can be seen that, for larger Reynolds numbers, the shape of the Nusselt number distributions is consistent with published data available in the literature. There exists a local minimum at the stagnation point and the heat transfer increases to a peak at $r/D = 0.7$ where the fluid has to accelerate to escape the lip of the jet. The surface heat transfer then

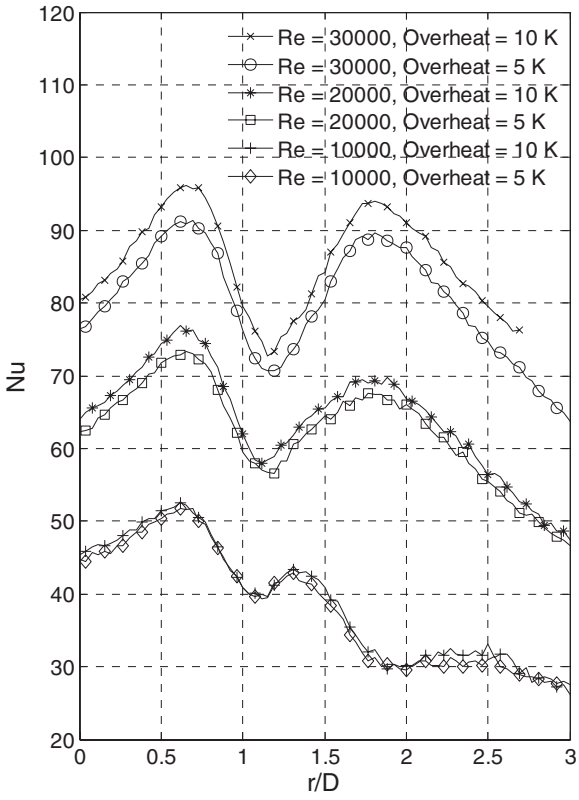

Figure 11. Effect of overheat on Nusselt number distributions: $H/D = 1.0$.

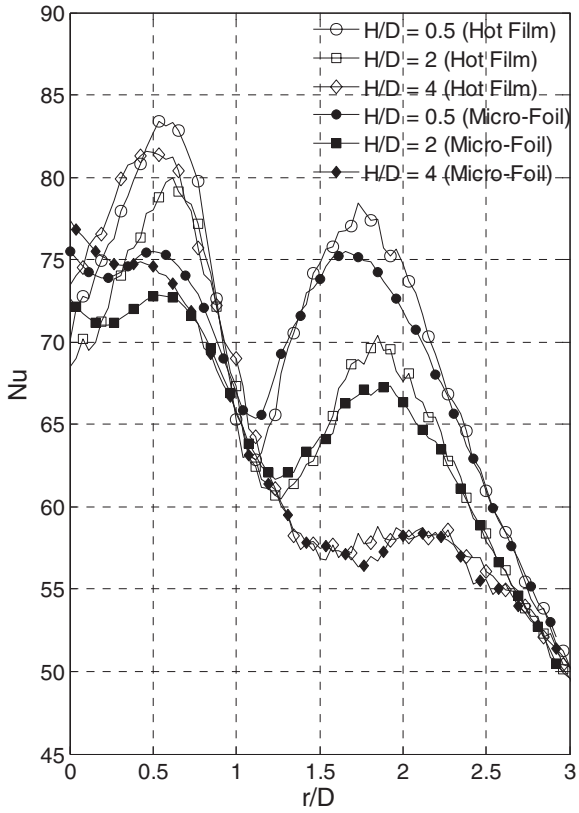

Figure 12. Nusselt number distributions using Micro-Foil® and hot-film sensors: overheat = 10 K and $Re = 20\,000$.

decreases as the boundary layer thickens before increasing again to a secondary peak at a radial location between $1.25D$ and $1.75D$, depending on the Reynolds number; this is due to an abrupt increase in wall jet turbulence. For Reynolds numbers of 20 000 and 30 000, the heat transfer decreases from this secondary peak with ever increasing radial distance. The tertiary peak occurs only at the lowest Reynolds number of 10 000. These data support the hypothesis that this secondary peak is due to the secondary buoyancy-driven flow created by the sensor overheat. There is a lower limit to the magnitude of the forced convective heat transfer coefficient that can be measured with this technique therefore.

Finally, to further validate the hot-film surface heat flux measurement technique, these data were compared to data acquired using a flush-mounted Micro-Foil® heat flux sensor. The experimental setup was otherwise identical. Data presented in figure 12 compare heat transfer distributions for a jet Reynolds number of 20 000 impinging at nozzle to impingement surface spacings of 0.5, 2 and 4 diameters. For the range of parameters tested, there is good agreement between the Micro-Foil® and the hot-film heat flux measurements.

Minor discrepancies between the two measurement techniques can be attributed to the spatial resolution differences and the relative disturbance caused by each of the sensors to the thermal boundary condition. In particular, the hot-film sensor data indicate a greater difference between the magnitude of the heat transfer in the trough (between the two peaks in heat transfer) and the magnitude of the peaks themselves. This indicates that the sensor has better spatial resolution than the Micro-Foil®, which has a larger sensor area and averages locally.

The difference in the shape and magnitude of the heat transfer distributions in the stagnation region is attributed to both the spatial resolution differences and the disturbance of the thermal boundary condition. At the stagnation point of the impinging jet flow, the hot-film records a local minimum at the stagnation point for the range of parameters tested, whereas the Micro-Foil® indicates that the heat transfer at the stagnation point is a local maximum. This is thought to be due, in part, to the poor spatial resolution of the Micro-Foil® heat flux sensor which is unable to detect steep gradients in the surface heat transfer such as occuring in the stagnation region. The disturbance of the boundary condition is also a factor; at the stagnation point the size of the Micro-Foil® and its influence on the thermal boundary condition is more significant, which results in artificially high values of heat transfer. Although the hot-film sensor operates using a heated element, the thermal mass of the hot-film element is small due to the physical size of the element. The correction technique also eliminates the bias error created by the presence of the sensor. The Micro-Foil®, however, consists of a relatively thick thermal barrier (0.2 mm Kapton). This contributes to a significant disturbance of the surface thermal boundary condition that results in discrepancies with the hot-film sensor measurements.

Overall, however, the magnitude of the differences between the two techniques is small, thus validating the

new hot-film measurement technique for surface heat transfer measurements.

5. Conclusions

An improved technique to measure surface heat flux has been presented. A flush-mounted hot-film sensor, working in conjunction with a CTA, has been shown to give accurate and repeatable surface heat flux measurements. These results are in good agreement with previous studies and experimental results achieved using a more established measurement technique.

It is necessary to maintain the hot-film sensor element at a temperature above that of the surface on which it is mounted. This has been shown to result in a bias error in the surface heat flux measurement. A technique to correct for this error has been established and successfully implemented.

A numerical model that demonstrates the thermal performance of the sensor in heated and adiabatic conditions has also been presented. The magnitude of the effective surface area calculated is broadly consistent with experimental findings. The magnitude of the effective surface area has been shown to decrease with increasing magnitude of the overheat. The connecting copper terminals are primarily responsible for the increased area. Since these sensors are not designed for this application of surface heat flux measurement and normally operate at higher overheats to measure wall shear stress, there is scope to improve the sensor design for heat flux measurement applications.

The magnitude of the overheat has been shown to directly influence the accuracy of the measurement technique. Larger magnitudes of the overheat disturb the thermal boundary condition and contribute to the magnitude of the measurement uncertainty. As the overheat increases, so too does the bias error measured during the adiabatic test. This amplifies the significance of the difference between the effective surface areas under the two test conditions. A large overheat also has the potential to cause a significant disturbance in the thermal boundary condition that will adversely affect the accuracy of the measurement. This has been demonstrated for instances where the local flow velocity is low. Careful design of the operating parameters is therefore required to ensure the hot-film technique produces accurate results. As indicated by the numerical model, the magnitude of the effective surface area is larger when operating under the heated condition than for the adiabatic condition. It is necessary to assume that this area is constant in practical use to apply the correction technique. This will also contribute to the uncertainty of the resulting measurement.

The uncertainty of the measurement technique is shown to decrease as the magnitude of the overheat tends towards zero. It is expected however, at very low values of the sensor overheat, that the signal to noise ratio would become insignificant as the power required to maintain the sensor at very low overheats approaches zero. The limiting value of the sensor overheat is the subject of future work in this area.

Overall, the hot-film technique has been shown to achieve surface heat transfer measurements that are accurate and with better spatial resolution than other, more established techniques. While this research has not focused on the temporal response of the technique, CTA can produce a response in the region of 100 kHz region for hot wire anemometry and flow velocity measurements. Issues relating to heat capacitance will significantly limit the temporal response of the technique and further research is required to ascertain the maximum frequency response.

References

[1] Albrecht H-E, Damaschke N, Borys M and Tropea C 2003 Laser Doppler and phase Doppler measurement techniques *Experimental Fluid Mechanics* (Berlin: Springer)

[2] Raffel M, Willert C E, Wereley S T and Kompenhans J 2007 *Particle Image Velocimetry—A Practical Guide* (Berlin: Springer)

[3] Bruun H H 1995 *Hot-Wire Anemometry—Principles and Signal Analysis* (Oxford: Oxford University Press)

[4] Ireland P T and Jones T V 1987 The response time of a surface thermometer employing encapsulated thermochromic liquid crystals *J. Phys. E: Sci. Instrum.* **20** 1195

[5] Golobic I, Petkovsek J, Baselj M, Papez A and Kenning D 2009 Experimental determination of transient wall temperature distributions close to growing vapor bubbles *Heat Mass Transfer* **45** 857–66

[6] Nakamura H 2009 Frequency response and spatial resolution of a thin foil for heat transfer measurements using infrared thermography *Int. J. Heat Mass Transfer* **52** 5040–5

[7] Hoogendoorn C J 1977 The effect of turbulence on heat transfer at a stagnation point *Int. J. Heat Mass Transfer* **20** 1333–8

[8] Gardon R J and Akfirat J C 1965 The role of turbulence in determining the heat transfer characteristics of impinging jets *Int. J. Heat Mass Transfer* **8** 1261–72

[9] Liu T and Sullivan J P 1996 Heat transfer and flow structures in an excited circular impinging jet *Int. J. Heat Mass Transfer* **39** 3695–706

[10] O'Donovan T S and Murray D B 2007 Jet impingement heat transfer: part I. Mean and root-mean-square heat transfer and velocity distributions *Int. J. Heat Mass Transfer* **50** 3291–301

[11] O'Donovan T S and Murray D B 2007 Jet impingement heat transfer: part II. A temporal investigation of heat transfer and local fluid velocities *Int. J. Heat Mass Transfer* **50** 3302–14

[12] Xie Q and Wroblewski D 1997 Effect of periodic unsteadiness on heat transfer in a turbulent boundary layer downstream of a cylinder–wall junction *Int. J. Heat Fluid Flow* **18** 107–15

[13] Beasley D E and Figliola R S 1988 A generalised analysis of a local heat flux probe *J. Phys. E: Sci. Instrum.* **21** 316–22

[14] Moen M J and Schneider S P 1994 The effect of sensor size on the performance flush-mounted hot-film sensors *ASME J. Fluid Eng.* **116** 273–7

[15] Scholten J W and Murray D B 1996 Measurement of convective heat transfer using hot film sensors: correction for sensor overheat *ASME J. Heat Transfer* **118** 982–4

[16] Hwang S D, Lee C H and Cho H H 2001 Heat transfer and flow structures in axisymmetric impinging jet controlled by vortex pairing *Int. J. Heat Fluid Flow* **22** 293–300

[17] Hwang S D and Cho H H 2003 Effects of acoustic excitation positions on heat transfer and flow in axisymmetric

impinging jet: main jet excitation and shear layer excitation *Int. J. Heat Fluid Flow* **24** 199–209

[18] Goldstein R J and Franchett M E 1988 Heat transfer from a flat surface to an oblique impinging jet *ASME J. Heat Transfer* **110** 84–90

[19] Shadlesky P S 1983 Stagnation point heat transfer for jet impingement to a plane surface *AIAA J.* **21** 1214–5

[20] Kim J H, Simon T W and Viskanta R 1993 Journal of heat transfer policy on reporting uncertainties in experimental measurements and results *ASME J. Heat Transfer* **115** 5–6

[21] Baughn J W, Hechanova A E and Yan X 1991 An experimental study of entrainment effects on the heat transfer from a flat surface to a heated circular impinging jet *ASME J. Heat Transfer* **113** 1023–5